# **Electrical Energy Generation using** Thermoelectric Modules and Plane Mirror Solar Collector

# Francis Onoroh 1,\*, Adeyinka Abdulguadri Oluwo 1, Nehemiah Sabinus Alozie 1

<sup>1</sup> Department of Mechanical Engineering, University of Lagos, Akoka, Yaba, Lagos Nigeria

Abstract: The negative effects of global warming resulting from an over-reliance on fossil fuels have been more apparent in recent times. The impending depletion of these resources is a significant threat to humankind's future. Thus, the necessity of creating safe, reliable, and sustainable energy sources is becoming more widely acknowledged. This research developed a solar thermoelectric generator using a plane mirror as a concentrator. The system consists of a plane mirror to concentrate sunlight, a receiver plate, TEG1-241-1.4-1.2 modules, a heat sink, a storage battery, and a power inverter. Temperature across the modules' interface was measured and is used to simulate the performance metric of thermal energy across the module surfaces, power, and efficiency of conversion. The setup yielded a maximum voltage of 13.7 V, a current of 1.8 A, a power output of 15 W, and an efficiency of 8%. The findings underscore the advantages of utilizing thermoelectric modules, particularly in harnessing waste heat. The outcomes of this study contribute to the growing body of knowledge on sustainable energy systems and provide insights for further optimization and implementation.

**Keywords:** Solar radiation; modules; current; voltage; power; efficiency.

#### 1. Introduction

The need for creative solutions for energy supply, conservation, and environmental protection is growing due to the world's rising energy consumption. Energy security must be prioritized for long-term economic development because it is essential to a nation's ability to prosper economically. Solar energy, an endless, renewable energy source, presents itself as a viable option for sustainable development [1][2]. Generally, solar energy can be converted into useful power in the form of photon or thermal energy [3]. Solar energy radiation captures the heat and radiant light from the sun, which is converted into electricity. Renewable energy sources provide environmentally favourable options, including biomass, solar, and wind power. It is projected that effective energy harvesting from these sources will be essential to provide humanity with clean energy alternatives.

Systems for concentrating solar power (CSP) provide a practical way to transform solar energy into electrical energy. Power towers, parabolic dishes, parabolic troughs, linear Fresnel reflectors, and plane mirrors are some of the CSP technologies that are being developed to capture solar energy [4]. Plane mirrors are readily available, cheap, and effective solar energy concentrators among them all. The hybridization of the thermoelectric generator and the solar plane mirror concentrator is then referred to as Solar Thermoelectric Generator (STEG). The extensive utilization of STEG systems encompasses the retrieval of various forms of waste heat, such as that from photovoltaic cells, automotive exhausts, light-emitting diodes, and industrial sources [5].

Thermoelectric generators (TEGs) are tiny direct energy conversion devices that

use the Seebeck effect to harness the temperature differential between their hot and cold sides to produce electricity. Because of their distinct benefits, which include zero emissions, solid-state and silent operation, lack of moving parts, excellent reliability. maintenance-free operation. thermoelectric generators (TEGs) are among the most alluring waste heat recovery technologies [6]. Thermoelectric materials are semiconductors made up of two distinct materials. Pairs of these materials, referred to as "couples," are layered between two ceramic substrates to form thermoelectric (TE) modules. Based on thermoelectric couplings (nand p-type semiconductor legs), these modules are soldered between the ceramic plates to form an electrical series connection and a thermal parallel connection [7]. The movement of electrons from the material's hot side to its cold side and vice versa is facilitated by the p-type and n-type materials. The temperature differential between the TEG and the Seebeck coefficient affects the resulting potential difference or voltage output, power production, conversion efficiency, and dependability used to evaluate its performance.

For a very long time, energy has been essential to the development of human civilization. Energy use increases in step with changes in human living standards. Since it plays a crucial part in a nation's economic development, maintaining energy security is essential for long-term economic success. The negative effects of global warming resulting from an over-reliance on fossil fuels have been more apparent in recent times. The impending depletion of these resources is a significant threat to humankind's future, even putting air pollution concerns aside. Thus, the necessity of creating safe, reliable, and sustainable energy sources is becoming more widely acknowledged.

Bakar et al. [8] worked on the theoretical model of a solar thermoelectric generator (STEG) for the generation of heat and power. In their study, a theoretical model accurately predicts STEG performance, validated through experimental data with differences between the theoretical model and experimental data less than 20%. It was found out that a 10° tilt gets more sunlight. The models, practical tests, and experimental results all support that STEG is a reliable way to produce both heat and electricity at the same time. Muhammed et al. [9] successfully demonstrated the fabrication

and performance evaluation of a prototype solar thermoelectric generator (STEG) using locally available materials. Their study was carried out experimentally, and the results obtained showed that the STEG, with its collector, captured 1.12 kW of sunlight, creating an average daily electric power of 11.8 mV with a temperature difference of 77.28°C and a resultant efficiency of 3%.

Acar and Bas [10] looked into the use of thermoelectric modules and focused photovoltaic panels for energy generation. The work investigates integrating a thermoelectric generator to increase photovoltaic efficiency. Determining material attributes, building a model, and implementing mixed convection and radiation boundary conditions are all part of the numerical solution. The hybrid concentrated photovoltaic thermoelectric generator (CPV-TEG) system performs better than the uncooled CPV, according to the results. It can operate at higher concentrations of solar radiation and achieve a notable increase in power production as well as a 20.45% improvement in overall system electrical efficiency. Algarni and Irshad [11] evaluated a flat plate solar collector and a hybrid thermoelectric generator. The findings demonstrate that adding TEGs to the solar collector's back improves performance and efficiency. The unique technique can generate 2.2 W of power at midday from leftover heat. The data and analysis from the study demonstrate that the addition of TEGs has an impact on electricity, temperature, and overall efficiency. Without requiring many power connections, this new method looks like a fantastic approach to implementing renewable energy.

Emad et al. [12] investigated the connection of a concentrated solar cell with a thermoelectric generator. Thermoelectric generators efficiently lower cell temperatures and improve energy generation when incorporated with concentrated photovoltaic (CPV) technology. When comparing the hybrid CPV-TEG to uncooled CPV systems, the results demonstrate that the hybrid system can operate at higher concentrations of solar radiation, maximizing power output to 1.433 W/cm<sup>2</sup>, with the TEGs serving as passive cooling systems. This results in a significant reduction of cell temperatures and an overall 10.45% improvement in system efficiency. Hashim et al. [13], in their study, investigate the potential of concentrating solar thermoelectric generators (CSTEGs) in generating

limited electricity. Exploring both experimental and numerical modelling approaches, it highlights the limitations of traditional thermoelectric generators (TEGs) and proposes enhancements through integration with concentrators or vacuum systems. Emphasizing the crucial need for effective heat absorption from TEG cells, they discussed cooling methods utilizing aluminium heat sinks or phase change materials. Ultimately, the study suggests that combining concentrator systems with TEGs holds promise for increasing both electricity and heat production efficiency.

Sahu et al. [14] conducted research on electricity generation using a solar parabolic dish system coupled with a thermoelectric generator. Their focus was on addressing the challenges posed by high electrical grid costs in rural India, proposing standalone solar solutions, particularly emphasizing the use of thermoelectric generators (TEGS) in conjunction with solar parabolic dish concentrators (SPDCs). The system's electrical output and energy conversion efficiency were assessed by experimental study. The findings showed a maximum effective electrical efficiency of 0.424% and a TEG conversion efficiency of 2.76%. Muthu et al. [2] measured operating parameters like solar radiation, electrical power, receiver plate temperature, heat sink temperature, and temperature difference while conducting a performance analysis of a solar parabolic dish thermoelectric generator that uses solar radiation to generate electricity. With four modules producing 23.6 W in clear sun with a receiver plate temperature of 120°C and 1100 W/ m2 of solar radiation, the results show the potential of TEG. The study offers recommendations for rural communities wishing to adopt sustainable energy solutions by highlighting the possibilities of thermoelectric systems in conjunction with concentrated solar power generation.

Fan et al. [3] investigated the use of a solar dish concentrator to generate electricity from thermoelectric cells. Under various heating rates, experimental testing was performed on both individual cells and the entire concentrated thermoelectric, CTEG, system. For a temperature differential of 109°C, a single TEG generator can generate 4.9 W at maximal heat flux, which translates to 2.9% electrical efficiency. With a hot-side temperature of 68°C and a temperature differential of 35°C, the entire (CTEG) system can generate up to 5.9 W of electricity. Recently, a lot of research has been done on innovative hybrid system configurations that use solar energy. These configurations, which include, among other things, thermoelectric generator modules, photovoltaic systems, phase change materials (PCM), and solar thermal collectors, are meant to minimize heat losses and maximize solar energy usage. This present research centred on the use of a plane mirror as a concentrator for electricity generation via thermoelectric modules.

#### 2. Materials and Methods

Solar radiation has the capacity to generate both heat and electricity. Solar irradiation incident on a plane mirror can be directed to strike a receiver plate on which thermoelectric modules are attached, with the plate acting as a thermal mass. A means of dissipating heat is then bolted to the assembly, maintaining the modules' surfaces at different temperatures. Figure 1 shows a schematic of the developed solar thermoelectric generator.

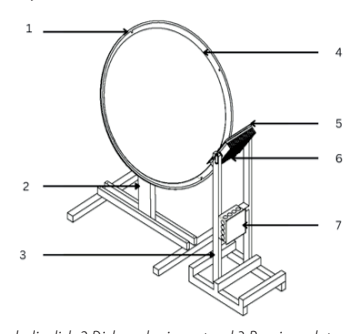
The useful heat generated by the plane mirror and incident on the receiver plate is obtained using Equation (1) [15]:

$$Q = \eta_o \times G_t \times A_n \tag{1}$$

Where  $\eta_0$  is the optical efficiency of the plane mirror;  $G_t$  is the solar radiation-striking surface of the plane mirror, W/m<sup>2</sup>; and  $A_p$  area of the plane mirror, m<sup>2</sup>. The solar radiation striking the surface of the mirror is as given in Equation (2) [16][17]:

$$G_t = G_{ND} + G_d + G_R \tag{2}$$

Where  $G_{ND}$ ,  $G_d$  and  $G_R$  represent the direct normal radiation, diffuse radiation and reflected radiation respectively, W/m<sup>2</sup>.



Part list: 1 Parabolic dish 2 Dish and mirror stand 3 Receiver plate modules, heat sink and switch box stand, 4 Plane mirror 5 Receiver plate 6 heat sink stand 7 Switch box

According to McQuiston et al. [16], the normal direct solar irradiation can be calculated using Equation (3):

$$G_{ND} = \frac{A}{exp\left(\frac{B}{\sin\beta}\right)} C_N \tag{3}$$

Where A is the apparent solar irradiation at air mass equal to zero, W/m²; B is the atmospheric extinction coefficient;  $\beta$  is the solar altitude, °;  $C_N$  is the clearness number. The solar altitude is obtained using Equation (4):

$$\sin \beta = \cos l \cosh \cos \delta + \sin l \sin \delta \tag{4}$$

Where l is the latitude, °; h is the hour angle, °; h is the declination, °. The hour angle and declination are obtain using Equation (5) and Equation (6), respectively:

$$h = 15(LST - 12) \tag{5}$$

$$\delta = 23.45 sin \left( \frac{360}{365} (284 + n_d) \right) \tag{6}$$

Where LST is the local solar time, obtained using Equation (7):

$$LST = \left(Local \, standard \, time\right) - \left(L_{L} - L_{s}\right) \frac{4 \, min}{\deg W} + EOT \tag{7}$$

Where  $L_L$  is the longitude, °;  $L_S$  is the Central Standard Time, °; EOT is the equation of time in minutes;  $n_d$  is the number of days of the year. The diffuse solar radiation is expressed using Equation (8):

$$G_d = G_{ND} \cos \theta \tag{8}$$

Where  $\theta$  is the angle of incidence,°. For a horizontal surface, Equation (9) is applied:

$$\cos\theta = \sin\beta \tag{9}$$

The reflected irradiation is obtained using Equation (10):

$$G_{R} = G_{ND} F_{LS} \left( \sin \beta + C \right) \tag{10}$$

Where  $F_{LS}$  is the surface configuration factor, and it is expressed using Equation (11):

$$F_{LS} = \frac{1 - \cos \alpha}{2} \tag{11}$$

Where lpha is the tilt angle of the surface, °. Table 1 depicts the numerical values of the solar data for

the computation of solar irradiation incident on the receiver plate for the months of August, September, October, November, and December. These variables are inputs into Equation (3) to Equation (11) respectively, to enable the solution of Equation (2).

Table 1: Solar Data for Twenty-First Day of Each Month [16]

Month of the Year	EOT, min	δ,°	A, W/m²	В	С
August	-2.4	12.3	1107	0.182	0.134
September	7.5	0.0	1136	0.165	0.121
October	15.4	-10.5	1166	0.152	0.111
November	13.8	-19.8	1190	0.142	0.106
December	1.6	-23.45	1204	0.141	0.103

In this research, twelve pieces of TEG1-241-1.4-1.2 modules were used to fabricate the thermoelectric generator. Figure 2 depicts a piece of the TEG1-241-1.4-1.2 module comprising 241 PN junctions, a 1.4 particle size cross-section area of the P and N junction and a 1.2 particle height of the P and N knot, having an open circuit voltage of 11.5 V. With a heat of 239 W, the output voltage and output current are 7 V and 1.25 A respectively as specified by ShenMingYang Electronics Ltd., the manufacturer of the modules. The selection of this particular module hinges on the high particle height of the individual P knot and N knot and its ability to withstand a temperature of 200°C. The modules were connected in four parallel strings to yield a designed output current of 5 A and output voltage of 21 V. The plane mirror is used to concentrate solar radiation onto the receiver plate of the hot side of the thermoelectric modules, as they are common and less costly compared to concave and convex mirrors.



Figure 2: Thermoelectric Module sample

Equations (12) and (13) represent the amounts of heat that must be supplied and rejected at the modules' hot and cold sides, respectively [18]:

$$Q_h = n\alpha T_h I + nK \left( T_h - T_c \right) - \frac{1}{2} I^2 nR \tag{12}$$

$$Q_{c} = n\alpha T_{c}I - nK\left(T_{h} - T_{c}\right) - \frac{1}{2}I^{2}nR \tag{13}$$

Where  $T_h$  and  $T_e$  are the hot side and cold side temperatures respectively, in °C, I is the output current of the thermoelectric generator, in A; K is the thermal conductance, in W/K; R is the internal resistance of the modules, in  $\Omega$ . The Seebeck coefficient, electrical resistivity and thermal conductivity are functions of temperature, which can be approximated using Equation (14), Equation (15), and Equation (16) respectively [14]:

$$\alpha = (22224 + 930.6T_{av} - 0.9905T_{av}^{2}) \times 10^{-9}$$
 (14)

$$\rho = (5112 + 163.4T_{av} - 0.6279T_{av}^{2}) \times 10^{-10}$$
 (15)

$$k = (62605 - 277.7T_{av} + 0.4131T_{av}^{2}) \times 10^{-4}$$
 (16)

Where the average temperature across the module can be calculated using Equation (17) [9]:

$$T_{av} = \frac{T_h + T_c}{2} \tag{17}$$

The product of internal resistance and thermal conductance is approximated for a thermocouple using Equation (18) [19]:

$$KR = \left(2\sqrt{k\rho}\right)^2 \tag{18}$$

The figure of merit of the thermoelectric couple is then obtained using Equation (19) [20]:

$$z = \frac{\alpha^2}{KR} \tag{19}$$

The characteristics of a thermocouple are embedded in the figure of merit; the greater the value of z, the greater the efficiency. The load resistance is related to the internal resistance of the thermoelectric modules using Equation (20):

$$R = \frac{R_L}{m} \tag{20}$$

The parameter m is obtained from Equation (21):

$$m = \sqrt{1 + T_{av}z} \tag{21}$$

The voltage output of the thermoelectric generator is then obtained using Equation (22):

$$V_{teg} = V_{oc} - IR \tag{22}$$

The power output and efficiency of energy conversion of the thermoelectric generator are obtained from Equation (23) and Equation (24), respectively [21][22]:

$$P = Q_h - Q_c \tag{23}$$

$$\eta = \frac{P}{Q_b} \tag{24}$$

Heat sinks play a vital role for efficient thermal dissipation necessary for the establishment of a temperature gradient across the thermoelectric modules. Figure 3 depicts a sketch of a heat sink and its equivalent thermal resistance network. The thermal resistance of the heat sink is a function of the number, height, and thickness of fins; fin spacing; length and width of heat sink; and the base thickness.

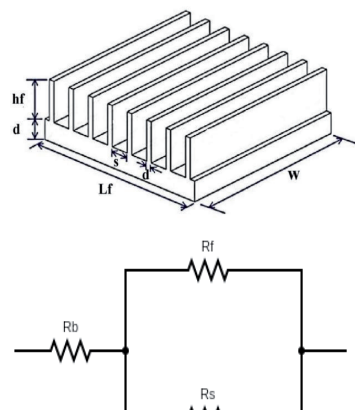


Figure 3: Heat sink and its thermal resistance

The thermal resistances of the base, fin and convection of the heat sink can be obtained using Equation (25), Equation (26), and Equation (27), respectively [23]:

$$R_b = \frac{d}{kwL_f} \tag{25}$$

$$R_f = \frac{h_f}{k t n} \times n_f \tag{26}$$

$$R_{f} = \frac{h_{f}}{ktw} \times n_{f}$$

$$R_{c} = \frac{1}{h((n_{f} - 1)(sw + 2h_{f}w))}$$
(26)

Where  $n_f$  is the number of fins; s is the fin spacing, m;  $h_f$  is the height of fin, m; t is thickness of fin, m;  $L_f$ is the length of heat sink, m; d is the heat sink base thickness, m; w is the width of heat sink, m; h is the heat transfer coefficient, W/m2K. The equivalent thermal resistance of the heat is computed using Equation (28) as:

$$R_{s} = \frac{wd\left[kt + n_{f}h_{f}\left(n_{f} - 1\right)\left(s + 2h_{f}\right)\right] + n_{f}h_{f}kwL}{w\left[\left(kL\right)\left(kt + n_{f}h\left(n_{f} - 1\right)\left(s + 2h_{f}\right)\right)\right]}$$
(28)

The Rayleigh number, Grashoff number, Prandtl number, and heat transfer coefficient can be calculated using Equation (29), Equation (30), Equation (31), and Equation (32), respectively [24] [25][26]:

$$Ra = Gr \times Pr \tag{29}$$

$$Gr = \frac{g\beta \left(T_s - T_\infty\right) L_h^3}{v^2} \tag{30}$$

$$\Pr = \frac{C_p \mu}{L} \tag{31}$$

The heat transfer coefficient is expressed as Equation (32):

$$h = \frac{Nuk_a}{L_b} \tag{32}$$

The coefficient of cubic expansion is approximated using Equation (33):

$$\beta = \frac{1}{T_{m}} \tag{33}$$

Where,  $T_s$  is the surface temperature, in °C;  $T_\infty$  is the ambient temperature, in °C; Lh is the hydraulic mean diameter, in m; g is the acceleration due to gravity, in m/s²; v is the kinematic viscosity of air, in m²/s;  $C_P$  is the specific heat capacity of air, in J/kgK;  $\mu$  is the dynamic viscosity of air, in N.s/m²;  $k_a$  is the thermal conductivity of air, in W/mK. Depending on the nature of flow of air, the Nusselt number is obtained using the appropriate form of Equation (34):

$$Nu = 0.54Ra^{\frac{1}{4}} \qquad 10^{4} < Ra < 10^{7}$$

$$0.15Ra^{\frac{1}{3}} \qquad 10^{7} < Ra < 10^{11}$$
(34)

The hydraulic mean diameter is expressed using equation (35):

$$L_h = \frac{2(h_f \times s)}{(h_f + s)} \tag{35}$$

# 3. Methodology

A model of a thermoelectric generator was designed and tested. The setup consists of a plane mirror mounted on a parabolic dish, TEG1-241-1.4-1.2 thermoelectric modules in a series and parallel arrangement, storage batteries, a receiver plate, a heat sink with a cooling fan, 40 A charge controller model EL2440Z, a switch box, a 12V 2.5-kVA power inverter. The heat sink was modelled and its thermal performance was investigated with ANSYS Fluent.

Temperature across the surface of the receiver plate and heat sink was monitored with time using the MTM-380SD reader. The performance of the thermoelectric generator was simulated using MATLAB to visualize the variation of the heat supplied and rejected, power, efficiency, current, and voltage output with the time of day. The constructional details of the thermoelectric generator are as shown in Figure 4, revealing the soldering and attachment of the modules to the receiver plate using a thin layer of thermal paste. The thermal paste significantly improves the receiver plate and heat sink performance by filling microscopic air gaps between the module and receiver plate on one hand and between the modules and heat sink on the other hand, creating a more complete, efficient pathway for heat to transfer due to reduction in thermal resistance. The receiver plate and modules array is screw firmly to the heat sink. The assembled receiver plate, modules, heat sink, and cooling fan are as shown in Figure 5. The electrical circuit of the setup is as shown in Figure 6. While Figure 7 detailed the experimental setup.

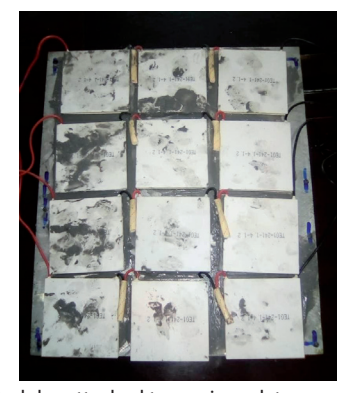


Figure 4: Modules attached to receiver plate



Figure 5: Assembly of Receiver plate, modules heat sink and cooling fan

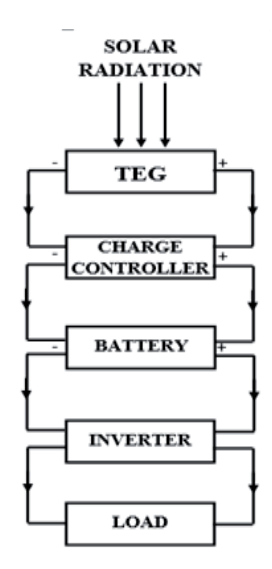


Figure 6: Setup Circuit Diagram

## 4. Results and Discussion

## 4.1 Thermal distribution across the receiver plate, module and heat sink

The mathematical model of the heat sink is optimized for the number of fins, fin spacing, fin thickness, and fin height, with the module arrangement fixing the length and width of the heat sink. The optimization tool in MATLAB, FMINCON, was used to obtain the heat sink geometry by setting lower and upper bound constraints considering the

volume of heat sink material. Table 2 detailed the optimized heat sink variables.

Effective thermal management is critical to ensuring the longevity and performance of the thermoelectric modules. The key metric for evaluating the effectiveness of a heat sink is its thermal resistance; it quantifies the heat sink's efficiency in transferring heat away from the thermoelectric modules to the surroundings. Higher efficiency of the heat sink results in higher temperature gradient across the thermoelectric modules, resulting in a flow of charge carriers from the n-type leg to the p-type leg, creating a higher voltage and current output. A heat sink with low thermal resistance provides higher power. Thus, the optimized heat sink with a thermal resistance of 0.4767 °C/W will enhance the performance and reliability of the thermoelectric generator. The thermal performance of the heat receiver plate, thermoelectric modules, and heat sink was simulated using CFD ANSYS Fluent using the average value of heat flux incident on the receiver plate.

Figure 8 depicts the assemblage of the receiver plate, modules, and heat sink modeled using Inventor and imported into ANSYS Fluent. The mesh created for the model in ANSYS demonstrates. a structured and uniform distribution. The use of hexahedral elements ensures high accuracy while maintaining computational efficiency. The mesh is

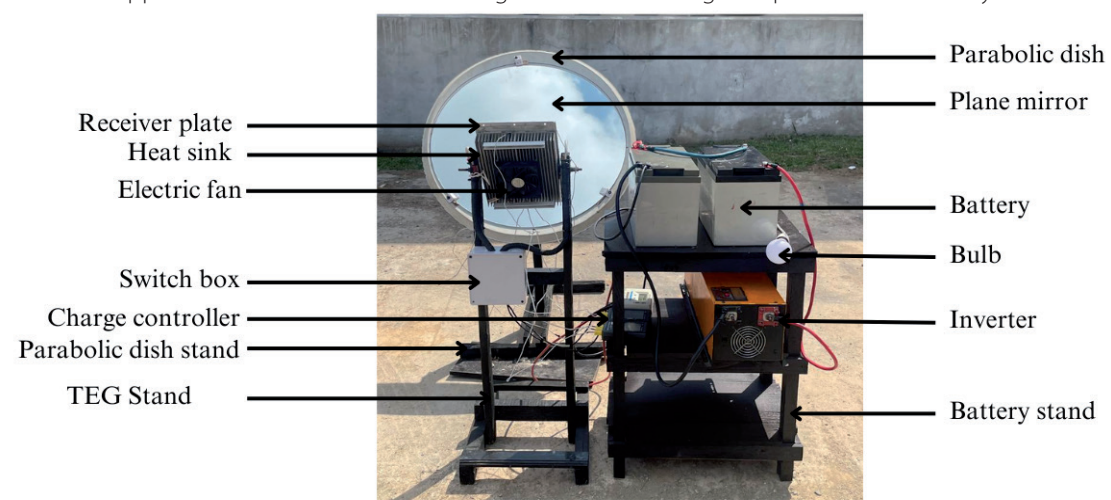


Figure 7: Experimental setup Table 2: Heat Sink Variables

Fin number	Fin height	Fin thickness	Fin spacing	Heat sink base thickness	Heat sink length	Heat sink weight	Thermal resistance
25	20 mm	4 mm	5 mm	6 mm	210 mm	210 mm	0.4767 °C/W

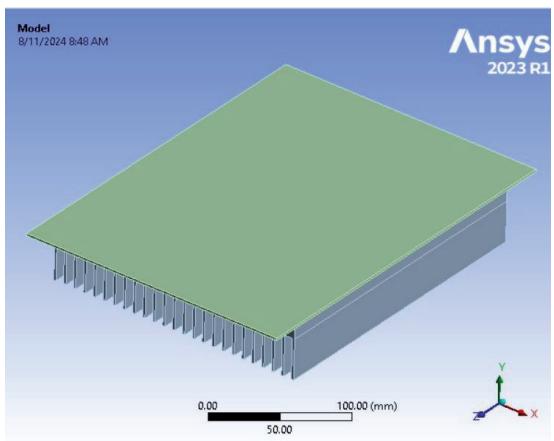


Figure 8: Model of Receiver plate, modules and heat sink

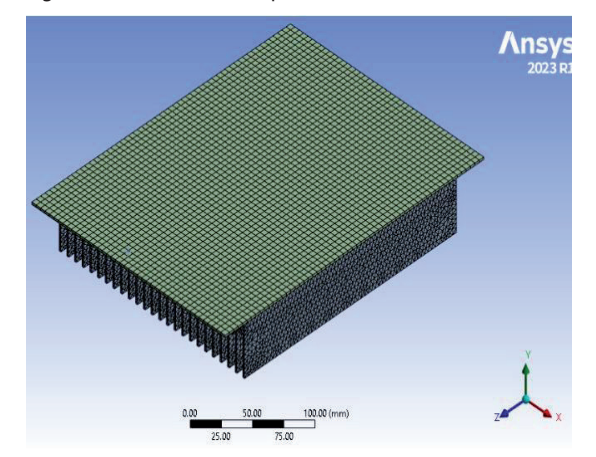


Figure 9: Meshed model of Receiver plate, Modules and heat sink

particularly dense around the fins, indicating careful consideration of areas where precise analysis is required. The mesh was generated using an element size of 0.0000208 mm, 60565 nodes and 159919 elements. Figure 9 shows the meshed assemblage of receiver plate, modules, and heat sink. After the mesh is checked and quality is guaranteed, the solver setup is activated to generate the thermal distribution shown in Figure 10 at an ambient temperature of 35°C and a heat flux of 640 W/m².

The thermograph illustrates the temperature distribution across the surface of the receiver plate, modules, and heat sink. The highest temperature, approximately 53.134°C, is observed at the top of the receiver plate. As heat is conducted through the modules, the temperature gradually decreases, reflecting the conversion of heat into electricity, with the heat sink having a minimum temperature of 38.205°C.

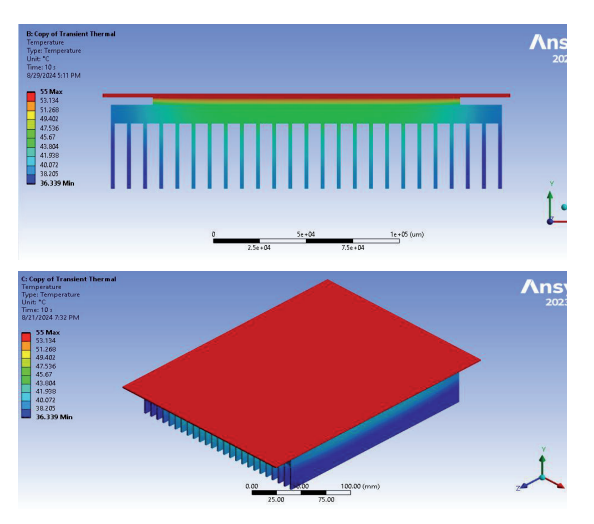


Figure 10: 2D and 3D thermograph of the receiver plate, modules and heat sink.

#### 4.2 Graph of temperature and solar intensity against time

Figure 11 shows the graph of the thermoelectric generator receiver plate and heat sink temperature as well as the sun intensity with time for the month of August 2024. The temperatures and solar intensity vary dynamically with time as expected due to changes in weather conditions, a trend also observed by Muthu et al. [2], Bamroongkhan et al. [4], Algami and Irshad, [11], and Shanmugam et al. [27]. As expected an increase in solar radiation results in a corresponding increase in the receiver plate temperature, establishing a temperature differential across the thermoelectric module interface responsible for the migration of electrons from the n-type leg to the p-type leg of the thermoelectric module. Higher temperature increases electron concentration density, leading to an enhanced mobility of electrons, which imparts voltage output.

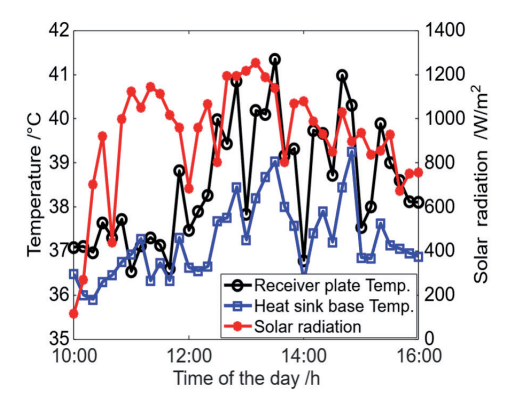


Figure 11: Temperature, solar intensity vs time of the day

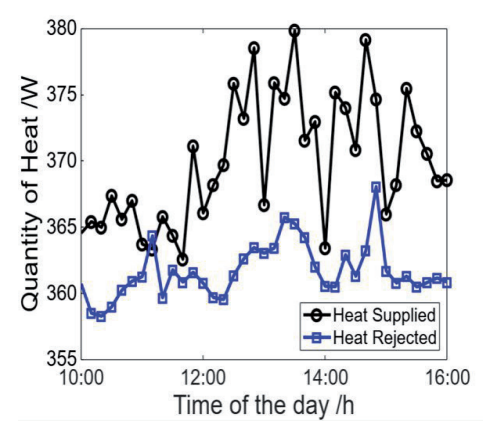


Figure 12: Heat supplied and rejected across the modules vs time of the day

#### 4.3 Graph of Heat against Time

Figure 12 shows how heat supplied to and heat rejected from the thermoelectric generator vary with time; Bakar et al. [8] reported similar results. The simulated thermal energy supplied and rejected are based on the data of Figure 11. An increase in solar radiation results in higher temperatures at the module's hot surface, which in turn leads to a higher heat supply. A thermoelectric generator has the ability to generate a higher amount of electrical power because of increased heat flow resulting from a larger temperature differential. The area between the heat supplied and heat rejected curves gives insights into the system's efficiency, as it represents the portion of heat that is effectively converted into electrical energy.

## 4.4 Graph of Power and Efficiency against Time

Figure 13 shows power and efficiency variation with time. The wavy pattern of fluctuation can be observed due to the unsteady nature of atmospheric conditions. Shittu et al. [6], Sahu et al. [14] and Shanmugan et al. [27], reported a similar trend. The simulation was carried out using the data of Figure 12. Increase in solar radiation incident on the receiver plate results in corresponding increase in temperature and heat supply that results in high power output. The system achieves a maximum power of 15 W and an efficiency of 8%.

## 4.5 Experimental Voltage and Current against Time

Figure 14 shows how the experimental current and voltage output vary with time. The unstable nature of the current and voltage is a result of the variation of the solar radiation incident on the receiver plate, which gives rise to irregular temperature gradients and heat supplied and

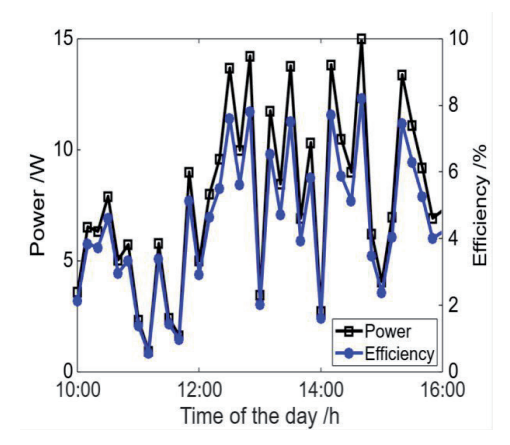


Figure 13: Power and Efficiency vs Time of the day

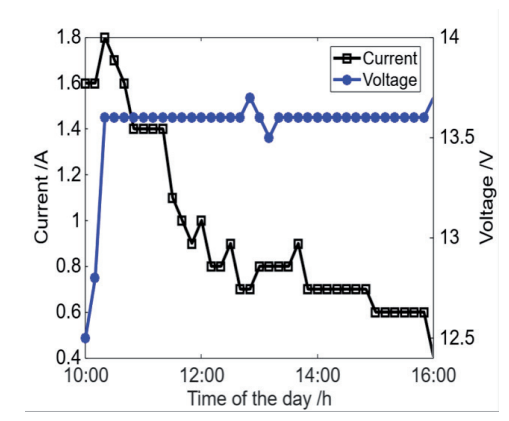


Figure 14: Voltage and Current against Time

rejected to the thermoelectric modules. Muhammad et al. [9], also report a similar pattern of results. The battery voltage rises from 12.5 V to a maximum value of 13.7 V and remains constant due to the action of the charge controller to prevent overcharging. The charge controller also prevents the battery from discharging through the thermoelectric modules. A maximum current of 1.8 A is obtained from the setup.

## 5. Conclusion

This research focused on generating electricity by combining solar energy with thermoelectric modules. The system uses a plane mirror, receiver plate, heat sink, and thermoelectric modules to harness solar radiation and convert it into electricity, which is then stored in a battery. Temperature across the receiver plate and heat sink was recorded to simulate heat transfer across the receiver plate and heat sink, power, and efficiency of electrical energy generation while monitoring the solar radiation.

Results of the experiment show attenuation of current and voltage with time, which is due partly to variation in atmospheric conditions and operation of a charge controller to safeguard the battery from overcharging yielding a maximum voltage of 13.7 and a 1.8 A current output, respectively. Thus, the system was able to charge the 12 V battery, demonstrating the feasibility of generating electricity from solar energy using a plane mirror as a concentrator and thermoelectric modules and a heat sink due to temperature differential. This research contributes to the growing field of renewable energy technologies, especially in the areas of application of thermoelectric generators for waste heat recovery. The combination of a plane mirror and thermoelectric generator offers a cost-effective and simple solution for solar energy harvesting, which can be applied in regions with epileptic electrical supply and in rural areas that are off the national grid. Despite the availability of literature, little effort has been committed to maintaining a constant temperature gradient across the module surfaces, necessitating further work in this regard using phase change material.

# References

- Sahu S. K.; Kopalakrishnaswami S. A. and Natarajan S. K (2020). Design and development of a low-cost solar parabolic dish concentrator system with manual dual-axis tracking. International Journal of Energy Research, 45(1).
- Muthu G.; Thulasi S.; Dhinakaran V. and Mothilal T (2020).
   Performance of solar parabolic dish thermoelectric generator with PCM. Materials Today Proceedings, 37, 929-933.
- Fan H.; Singh R. and Akbarzadeh A (2021). Electric Power Generation from Thermoelectric Cells Using a Solar Dish Concentrator. Journal of Electronic Materials, 40(5), 1312-1320
- Bamroongkhan P.; Lertsatitthanakorn C.; Sathapornprasath K. and Soponronnarit S. (2021). Experimental performance of a photovoltaic-assisted solar parabolic dish thermoelectric system, Case Studies in Thermal Engineering, 27, 101280, 1-9.
- Nyandang A. N.; Singh B.; Remeli M. F. and Oberoi A (2021).
   Power Generation using Thermoelectric Power Generator with Parabolic Solar Dish Concentrator, Journal of Physics: Conference Series, 012004, 1-14.
- Shittu S.; Li G.; Zhao X.; Zhou J.; Ma X. and Akhlaghi Y. G (2020). Experimental study and exergy analysis of photovoltaic-thermoelectric with flat plate micro-channel

- heat pipe, Energy Conversion and Management, 207, 1-11.
- Eswaramoorthy M. and Shanmugam S (2013). Solar Parabolic Dish Thermoelectric Generator: A Technical Study, Energy Sources, Part A: Recovery, Utilization, and Environmental Effects, 35(5), 487-494.
- 8. Bakar R. A.; Singh B. S.; Remeli M. F. and Ong K. S. (2021). Theoretical model of solar thermoelectric generator for heat and power generation, IOP Conference Series Earth and Environmental Science, 685, 1-10.
- Muhammad U. K.; Umar S.; Musa M. and DanShehu B. G. (2015). Fabrication and Performance Evaluation of a Prototype Solar Thermolectric Generator, Nigerian Journal of Solar Energy, 26, 43-50.
- Acar B. and Bas S. (2018). Investigation of energy generation at test system designed by use of concentrated photovoltaic panel and thermoelectric modules, International Journal of Renewable Energy Research, 8(4), 1859-1867.
- Algarni S. and Irshad K. (2023). Performance evaluation of a hybrid thermoelectric generator and flat plate solar collector system in a semi-arid climate, Case Studies in Thermal Engineering, 44, 102842, 1-8.
- Emad O.; Emam M.; Abdelrahman M. A. and Attia A. A. A. (2022). Studying the coupling of a concentrator photovoltaic cell with thermoelectric generator, Journal of Al-Azhar University Engineering Sector, 17(63), 577-587.
- Hashim H. T.; Rashid F. L. and Kadham M. J. (2021). Concentration solar thermoelectric generator, Journal of Mechanical Engineering Research and Developments, 44(1), 435-443.
- Sahu S. K.; Kopalakrishnaswami S. A. and Natarajan S. K. (2021). Electricity generation using solar parabolic dish system with thermoelectric generator-An experimental investigation, Heat Transfer, 50(8), 7784-9997.
- Kumar A.; Pachauri R. K. and Chauhan Y. K. (2015). Analysis
  and performance improvement of solar PV system by solar
  irradiation tracking, International Conference on Energy
  Economics and Environment (ICEEE), Greater Noida, India,
  1-6.
- McQuiston F. C.; Parker J. D. and Spitter J. D. (2005). Heating, Ventilating and Air Conditioning Analysis and Design (6th ed.), United States of America, John Wiley and Sons. Inc.
- Duffie J. A. and Beckman W. A. (1980). Solar Engineering of Thermal Processes (2nd ed.), New Jersey, John Wiley and Sons Inc.
- Abdelkefi A.; Alothman A. and Hajj M. R. (2013). Performance Analysis and Validation of Thermoelectric Energy Harvesters, Smart Materials and Structures, 22, 1-9.
- 19. Enescu D. (2019). Green Energy Advances, IntechOpen,
- 20. Da-Rosa A. V. and Ordonex J. C. (2021). Fundamental of

- Renewable Energy Processes (4th ed.), United States of America, Elsevier Academic Press.
- 21. Lertsatitthanakorn C.; Jamradloedluk J. and Rungsiyopas M. (2014). Electricity Generation from a Solar Parabolic Concentrator Coupled to a Thermoelectric Module, Energy Procedia: 2013 International Conference on Alternative Energy in Developing Countries and Emerging Economies, 52, 150-158.
- 22. Rowe D. M. (2006). Thermo-electrics Handbook Nano to Macro, New York, CRC press Taylor and Francis group.
- 23. Elghool A.; Basrawi F.; Ibrahim T. K.; Habib K.; Ibrahim H. and Idris D. M. N. (2017). A review on heat sink for thermo-electric power generation: Classifications and parameters affecting performance, Energy Conversion and Management, 134, 260-277.
- 24. Cengel, Y. A. (2006). Heat and mass transfer. A practical approach. (3rd ed.), New York, McGraw-Hill.
- 25. Sukumar R. S; Sriharsha G.; Arun S. B.; Kumar P. D. and Naidu C. (2013). Modelling and Analysis of Heat Sink with Rectangular Fins having through Holes, International Journal of Engineering Research and Applications, 3(2), 1557-1561.
- 26. Reddy M. C. S. (2015). Thermal Analysis of a Heat Sink for Electronics Cooling, International Journal of Mechanical Engineering and Technology, 6(11), 145-153.
- 27. Shanmugam S.; Veerappan A.; Eswaramoorthy M. (2014). An Experimental Evaluation of Energy and Exergy Efficiency of a Solar Parabolic Dish Thermoelectric Power Generator, Energy Sources, Part A: Recovery, Utilization, and Environmental Effects, 36(17), 1865-1870.

